O_2 and C O_2 Activation

Metalloenzymes play a vital role in metabolism; in particular, they are capable of functionalizing difficult substrates. These processes are remarkable because these transformations proceed with unprecedented level of regio-, chemo- and stereospecificity and, more importantly at mild conditions that can be hardly achieved by any industrial processes. Understanding the catalytic mechanisms of enzymatic reactions at the atomic level will enhance our knowledge for further design and synthesis of novel environmentally benign catalysts. Quantum chemical calculations contribute key information to this important field of investigation.

1. Calculation of the spectroscopic parameters of potential reaction intermediates and comparison with experimentally determined properties is vital for the structural identification of short-lived species that are inaccessible to X-ray crystallography.
2. Optimization of the structures of transition states in order to “connect” important intermediates and to predict reaction rates and kinetic isotope effects.
3. Qualitative analysis of the electronic structures of the intermediates and transition states provides deep chemical insights into catalytic mechanisms and complicated electron transfer processes.

The combined theoretical and spectroscopic analyses trigger new ideas for conclusive experiments that probe the intricate details of the catalytic mechanisms.

O_2 Activation

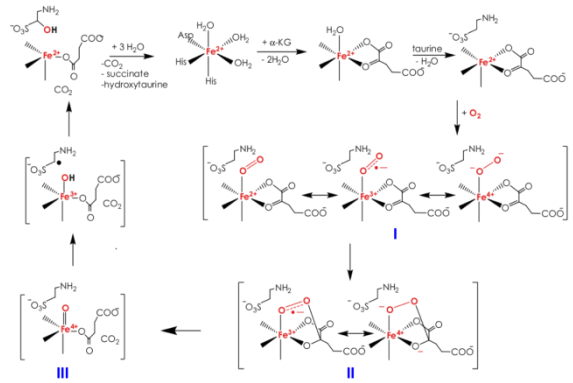

Scheme 1. Proposed consensus mechanism of the Fe(II)- and αKG-dependent dioxygenases.

Metalloenzymes can catalyze a range of oxidation reactions utilizing an ultimate "green" oxidant, dioxygen. The reactions are typically initiated by O2 binding at a reduced, electron-rich metal center, such as Cu(I) or Fe(II). The resulting dioxygen adducts often contain a coordinated superoxide.1 Subsequent reduction of O2 takes place along a well-defined reaction pathway and leads to formation of metal-peroxo and -oxo intermediates. More importantly, nature has developed various enzymes to employ all reduced forms of O2 to functionalize substrates.2

The Fe(II)- and α-ketoglutarate (αKG)-dependent dioxygenases serves as a representative example.3 The proposed mechanism (Scheme 1) involves (1) addition of dioxygen to the square pyramidal quaternary enzyme-Fe(II)-alpha-KG-substrate complex to yield an Fe(III)-superoxo intermediate (I), (2) attack of the uncoordinated O-atom in the O2-moiety on C2 of alpha-KG to form a bicyclic alkylperoxo species (II), (3) cleavage of the O-O bond and decarboxylation resulting in an Fe(IV)-oxo species (III),4 (4) abstraction of an H-atom from the substrate to yield an Fe(III)-hydroxide complex and a substrate radical, (5) hydroxylation via OH rebound, and (6)

dissociation of the product. We have employed high-level electronic-structure theory and spectroscopic tools to understand the reactivity of high-valent iron species.5

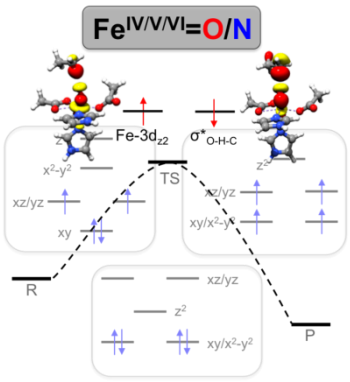

Fig. 1 An illustration of electronic structure and reactivity of synthetic high-valent iron complexes.

Synthetic oxo- and nitrido-iron complexes feature various coordination geometries and distinct electronic structures, and therefore exhibit diverse reactivity (Figure 1).6 Synergy from both experimental and theoretical findings can help us to elucidate their bonding and delineate their mechanistic features toward a range of chemical processes, like hydrogen-atom abstraction (HAT),7 oxygen atom transfer (OAT) and electron transfer (ET). In collaboration with Eckhard Bill, we employ various spectroscopic techniques to understand their bonding and electronic structure. Specifically, electron paramagnetic resonance (EPR), Mössbauer and magnetic circular dichroism (MCD) are in the front line of our current research. The MCD spectroscopy, in particular, is an outstanding technique because it is able to provide information about the geometric and electronic properties of the ground state such as oxidation and spin states, spin Hamiltonian parameters and coordination geometry as well as those of excited states. Thus, MCD serves as an invaluable link between ground state spectroscopy, EPR and excited state spectroscopy, electronic absorption (ABS) and resonance Raman spectroscopy.

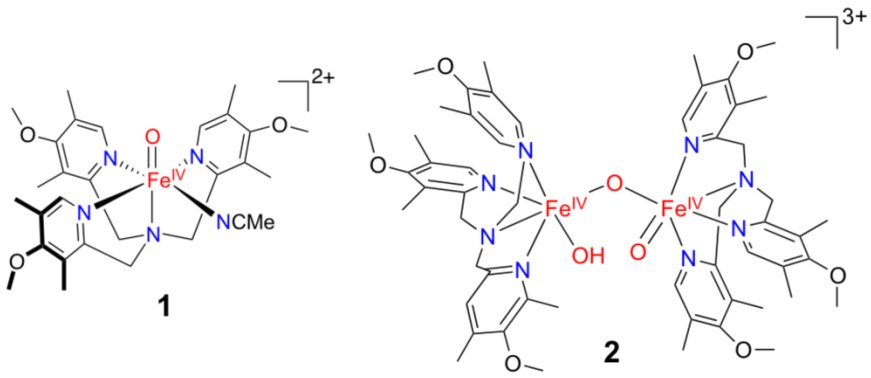

Scheme 2. Representative mononuclear (1) and binuclear (2) oxo-iron(IV) complexes.

A wealth of mononuclear oxo-iron(IV) model complexes have been prepared and characterized in the past decades, for which complex 1 serves as a representative example (Scheme 2). However, synthetic analogs of high-valent diiron species are still quite rare. Recent experiments report that a complex with a [FeIV2(μ-O)2] diamond core structure could be generated from open-core diiron(IV) complex 2 (Scheme 2) upon treatment with one equivalent of a strong acid. We performed a detailed MCD study on complexes 1 and 2 in combination with multi-configurational CASSCF/NEVPT2 (complete active space self-consistent field/N-electron valence perturbation theory) calculations to correlate their electronic structure and reactivity.8

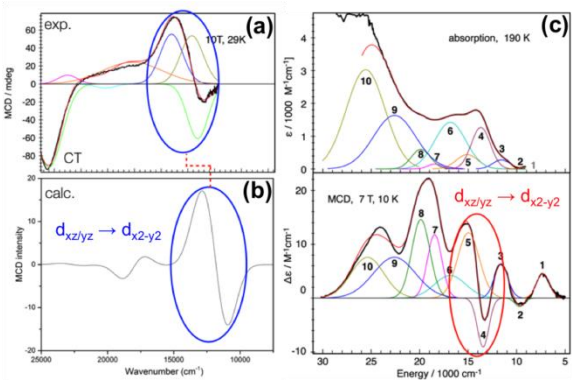

Fig. 2 MCD spectra of complex 1: (a) experimental (b) calculated. (c) Electron absorption and MCD spectra of complex 2.

The MCD spectra were directly calculated using CASSCF/NEVPT2 method and independent determination of the MCD signs were made based on the associated electron donating orbital (EDO) and electron accepting orbital (EAO) for a given transition. In comparison with experiment, this approach allowed us to make unambiguous assignments of the important transitions of complex 1 and gain more insight into the MCD signs and the temperature-dependent intensity variations (Figure 2a and 2b). Based on MCD/ABS intensity ratios, calculated excitation energies, polarizations, and MCD signs, the key transitions of complex 2 are assigned as ligand-field- or oxo- or hydroxo-to-metal charge transfer transitions. The correlation of the electronic structures of complexes 1 and 2 with their reactivity toward C–H bond oxidation and O-atom transfer reveals that, despite a difference in nuclearity, the two ferryl sites actually have very similar electronic structures that led to similar reactivity (Figure 2c).

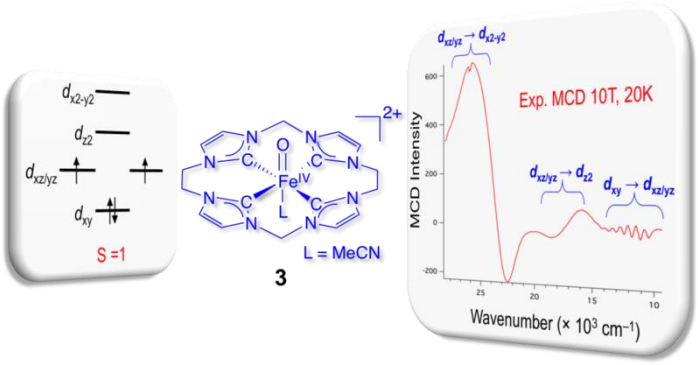

Fig. 3 Electronic structure and MCD spectra of a carbene-based oxo-iron(IV) complex.

We extended our understanding of electronic structure of oxo-iron(IV) complexes to a recently synthesized tetracarbene oxo-iron(IV) species (3) (Figure 3) using a combined experimental and theoretical approach.9 We were able to unambiguously assign the important ligand field transitions through direct computations of MCD spectra with CASSCF/NEVPT2 based methods and independent determination of the MCD C-term signs. In contrast to the majority of triplet ferryl complexes supported by polydentate N-donor ligands (complex 1), complex 3 has been proven to feature a distinct electron configuration in which the dx2-y2 orbital lies higher in energy than dz2. Our detailed electronic-structure analysis by using MCD and infrared photo dissociation (IRPD) spectroscopy clearly show that the tetracarbene ligand does not considerably affect the bonding in the (FeO)2+ core, but strongly destabilizes the dx2-y2 orbital and lifts it above the dz2 orbital in energy. As a result, the HAT reaction with complex 3 is likely to exclusively take place on the triplet surface due to the large quintet-triplet energy gap.

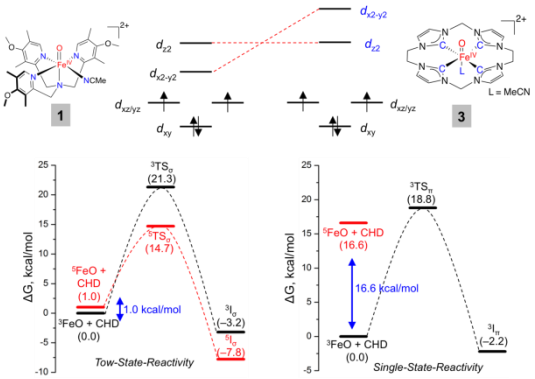

Fig.4 Comparison of the reaction profiles for complexes 1 and 3.

We have been performing theoretical investigation on the C–H activation reactivity exhibited by complexes 1, 2 and 3. The subtle difference in the electronic structures between complexes 1 and 3 results in a decisive consequence to their reactivity. Classical ferryl model compounds, such as complex 1, typically follow a mechanistic scenario of two-state reactivity for C-H bond activation. They usually have a low-lying quintet state (ΔG <3 kcal/mol,) with an electron configuration of (dxy)1(π*-dxz/yz)2(σ*-dx2-y2)1(σ*-dz2)0, and the quintet σ-pathway typically involves a much lower barrier than that for the triplet π-channel, the system hence first undergoes a spin-crossover to the quintet state and the subsequent C-H bond cleavage process takes place predominantly on the quintet surface. Due to swapping of the d-orbital energies in the eg set, the lowest-energy quintet state of complex 3 features an electron configuration of (dxy)1(π*-dxz/yz)2(σ*-dz2)1(σ*-dx2-y2)0. As a consequence, a significantly greater quintet-triplet energy separation (16.6 kcal/mol) is found for complex 3. Thus, the entire reaction is likely to exclusively occur on the triplet surface, viz. single-state reactivity (Figure 4). Our calculated barrier for the rate-determining step of H-atom transfer (18.8 kcal/mol) matches the experimental kinetic data (ΔG‡ (20° C) = 15.2 kcal/mol) very well, providing further credence to our proposed electronic structure.

CO_2 Activation

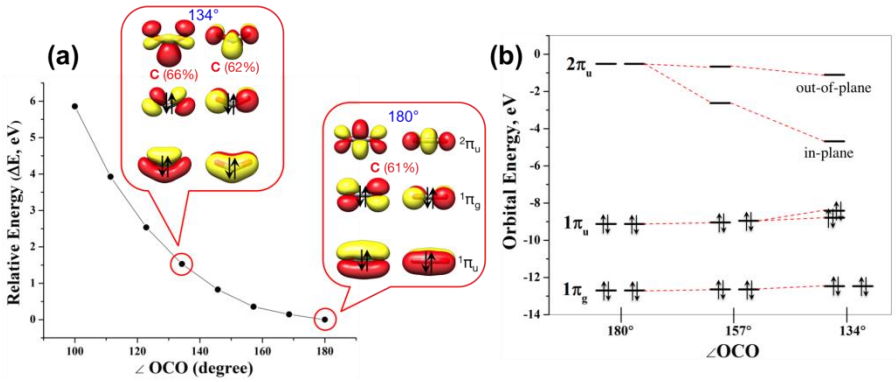

Fig. 5 (a) The change in the total energy as a function of OCO angle. (b) Molecular orbitals of CO_2 at different OCO angles.

Conversion of carbon dioxide into liquid fuels and useful chemicals has been the focus of energy research in recent decades. However, the transformation of CO_2 to value-added fine chemicals is challenging due to the high thermodynamic stability and kinetic inertness of CO_2.10 CO_2 features the highest oxidation state (+4) of carbon with a sufficiently negative one-electron reduction potential (-1.9 V). CO_2 bending results in lowering the energy of its Lowest Unoccupied Molecular Orbital (LUMO), resulting in an increased C p-orbital character in the LUMO while the Highest

Occupied Molecular Orbitals (HOMO) are O p-orbital centered (Figure 5). Thus C and O atoms are preferred sites for nucleophilic and electrophilic attacks. However, such geometric distortion leading to two-electron reduction requires high energy input and requires an efficient metal catalyst. CO_2 functionalization can take place either electrochemically or chemically, preferentially with a base-metal catalyst.

The homogeneous electrochemical reduction of CO_2 catalyzed by [Ni(cyclam)]+ occurs with high efficiency and selectivity yielding CO at a relatively low over-potential. By contrast, the same reaction occurring on mercury surface leads to a mixture of CO and formate. We propose CO to evolve from a η1-CO_2 adduct, whereas formate is likely to be generated from a η1-OCO intermediate.11 Our calculations predict the binding of CO_2 to [Ni(cyclam)]+ in a η1-C fashion to be a thermoneutral process while [Ni(η1-OCO)(cyclam)]+ is endoergic by 12.4 kcal/mol (Scheme 3). Hence it is presumed that the reaction pathway leading to formate formation is blocked at the initial phase of the homogeneous reaction.

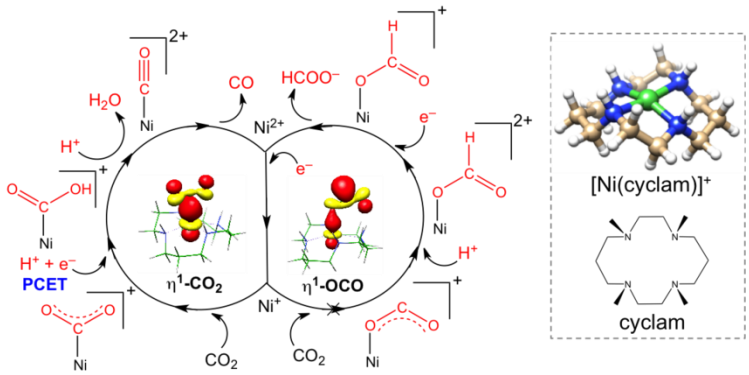

Scheme 3 The catalytic mechanism of CO_2 reduction by [Ni(cyclam)]+ (inside the circle: the molecular orbitals representing the Ni-CO_2 interaction).

Reduction of CO_2 to CO by low-valent metals typically entails CO_2 coordination and subsequent C–O bond cleavage. CO_2 binding to [Ni(cyclam)]+ only causes a partial electron transfer from Ni+ to CO_2, and the second electron transfer has to be achieved via an outer-sphere mechanism (Scheme 3). This reflects the inability of a single metal center to accommodate two readily accessible reducing equivalents, especially for 3d transition metals, which ultimately decreases the catalytic activity. We are currently working on similar mechanisms where one low-valent metal center serves as the electron donor and another metal center act as the Lewis acid to facilitate the electron transfer to CO_2. Alternatively, non-innocent ligands may function as more flexible and accessible electron reservoirs, because redox processes occurring on conjugated macrocyclic rings are likely to suffer from less reorganization energies than metal-centered redox events.12

CO_2 hydrogenation to formate or formic acid involves two key reaction steps, viz. base-promoted H_2-splitting (2 → 3) and hydride transfer (4 → 5) to CO_2 (Figure 6a), either of which can be the rate-determining step (RDS) of the overall catalytic cycle. We carried out a comparative mechanistic study on the reactivity of 1Fe, 1Co and 1Ru, and proposed that the hydride donation ability or the hydricity of the dihydride species (4) can dictate the nature of the RDS and modulate the RDS barriers.13 Recently, following this notion, a series of potential catalysts with differential hydricity have been designed (Figure 6b).14 We computationally evaluated their catalytic activity, and the results nicely correlate with our catalyst-design strategy. Specifically, enhancing the electron-donating power of high-hydricity catalyst lowers the barrier for the hydride-transfer RDS step. Conversely, the same modification leads to even greater barrier for

the H2-splitting RDS for low-hydricty catalyst. Finally, we could establish an elegant correlation between hydricity and barriers for the crucial steps (Figure 6c).

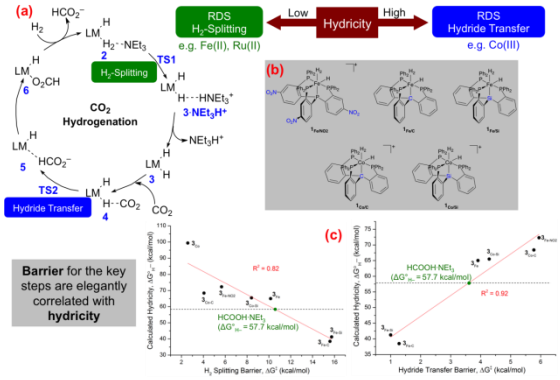

Fig. 6 CO_2 Hydrogenation to formate: (a) catalytic cycle, (b) newly designed species based on hydricity and (c) correlation plots between hydricity and barriers for crucial steps.

References

1. Tamanaha, E.; Zhang, B.; Guo, Y.; Chang, W.-C.; Barr, E. W.; Xing, G.; St Clair, J.; Ye, S.; Neese, F.; Bollinger, J. M., Jr.; Krebs, C. J. Am. Chem. Soc. 2016, 138, 8862–8874. (b) Wang, C.-C.; Chang, H.-C.; Lai, Y.-C.; Fang, H.; Li, C.-C.; Hsu, H.-K.; Li, Z.-Y.; Lin, T.-S.; Kuo, T.-S.; Neese, F.; Ye, S.; Chiang, Y.-W.; Tsai, M.-L.; Liaw, W.-F.; Lee, W.-Z. J. Am. Chem. Soc. 2016, 138, 14186–14189.
2. Christian, G. J.; Ye, S.; Neese, F. Chem. Sci. 2012, 3, 1600–1611. (b) Christian, G. J.; Neese, F.; Ye, S. Inorg. Chem. 2016, 55, 3853–3864.
3. Ye, S.; Riplinger, C.; Hansen, A.; Krebs, C.; Bollinger, J. M.; Neese, F. Chem. Eur. J. 2012, 18, 6555–6567.
4. Sinnecker, S.; Svensen, N.; Barr, E. W.; Ye, S.; Bollinger, J. M.; Neese, F.; Krebs, C. J. Am. Chem. Soc. 2007, 129, 6168–6179.
    a. Ye, S.; Geng, C.-Y.; Shaik, S.; Neese, F. Phys. Chem. Chem. Phys. 2013, 15, 8017–8030. (b) Ye, S.; Neese, F. Proc. Natl. Acad. Sci. U.S.A. 2011, 108 (4), 1228–1233. (c) Geng, C.; Ye, S.; Neese, F. Angew. Chem. Int. Ed. 2010, 49, 5717–5720. (d) Ye, S.; Neese, F. Curr. Opin. Chem. Biol. 2009, 13, 89–98.
5. Mondal, B.; Roy, L.; Neese, F.; Ye, S. Isr. J. Chem. 2016, 56, 763–772.
6. Geng, C.; Ye, S.; Neese, F. Dalton Trans. 2014, 43, 6079–6086.
7. Ye, S.; Xue, G.; Krivokapic, I.; Petrenko, T.; Bill, E.; Que, L., Jr; Neese, F. Chem. Sci. 2015, 6, 2909–2921.
8. Ye, S.; Kupper, C.; Meyer, S.; Andris, E.; Navrátil, R.; Krahe, O.; Mondal, B.; Atanasov, M.; Bill, E.; Roithová, J.; Meyer, F.; Neese, F. J. Am. Chem. Soc. 2016, 138, 14312–14325.
9. Mondal, B.; Song, J.; Neese, F.; Ye, S. Curr. Op. Chem. Biol. 2015, 25, 103–109.
10. Song, J.; Klein, E. L.; Neese. F.; Ye, S. Inorg. Chem. 2014, 53, 7500-7507.
11. Fang, H.; Jing, H.; Ge, H.; Brothers, P. J.; Fu, X.; Ye, S. J. Am. Chem. Soc. 2015, 137, 7122–7127.
12. Mondal, B.; Neese, F.; Ye, S. Inorg. Chem. 2015, 54, 7192–7198.
13. Mondal, B.; Neese, F.; Ye, S. Inorg. Chem. 2016, 55, 5438–5444.

Dr. Shengfa Ye, Theoretical Method Development, from website MPI CEC 2/2018